3. Development of high-content imaging of individual bacteria

3.1 Introduction

While there have been many recent startling advances in the field of bacterial genomics, it is arguable that there has not yet been a similar revolution in bacterial phenotyping. The phenotyping of clinical bacterial isolates relies primarily on empirical bacterial culture on agar plates, which in some cases is linked to rapid diagnostic tests, for example a urine dipstick[385]. Current assessment of minimum inhibitory concentrations of a drug to asses AMR in patients is largely performed by the use of semi-automated systems such as VITEK, or disk diffusion/ETESTs to measure the zone of inhibition of bacterial growth on a plate. While these strategies paired with genomic analysis can detect resistance in the overall population, they do not consider fluctuations within a bacterial population and likelihood of subtle mechanisms of drug evasion. To begin to tackle the deficiency in higher throughput microbial phenotyping, and potentially to obtain a faster and more accurate readout of bacterial behaviour under antimicrobial pressure, we investigated the use of high throughput microscopy for bacterial phenotyping.

With the advent of more powerful microscopy technologies, it is now possible to visualize and measure individual bacteria at high resolution to assess morphological characteristics. High-content imaging (HCI) is the combined technologies of high-resolution, high-throughput automated microscopy with automated analysis pipelines to derive meaning from the imaging data[386,387]. The ability to study individual bacteria and record changes allows for not only the assessment of bacterial response to antimicrobials but also the ability to screen novel compounds for efficacy and/or impact. Imaging has been used widely as a strategy to screen for drug impact on the behaviour of eukaryotic cells, and in theory similar principles can now be applied to antibacterial drug screening[388–392]. HCI has previously been used to study intracellular pathogens such as *Mycobacterium tuberculosis* and *Salmonella* species[393–397]. However, much of this work has been conducted looking at intracellular bacterial dynamics, and the screening of individual bacteria at scale is a much more recent phenomenon[398,399].

The strategy of imaging bacteria at high-throughput builds upon existing low-throughput strategies of capturing and analysing bacteria by microscopy. An assay for bacterial cytological profiling (BCP) has been developed in recent years by Pogliano and colleagues, facilitating the identification of morphological changes of bacteria after antimicrobial perturbation[359,400]. They used confocal microscopy to distinguish between bacteria exposed to five different classes of antimicrobials and subsequent image analysis could separate them into distinct clusters based on the drug mechanism of action[359,401]. Importantly, they showed that such imaging and analysis was applicable across multiple bacterial species, including *E. coli*, *Acinetobacter baumanii*, and *Staphylococcus aureus*[360,401–405].

Independently, there have been many efforts over the years to image bacteria individually and track movement and population expansion, particularly inside host cells[406,407]. However, one drawback with current low-throughput methodologies is that they require a pre-existing understanding of the phenotype in question to follow a discrete population or behaviour. In contrast, an agnostic approach to capturing all possible populations and phenotypic variants using HCI would be an important step towards better understanding bacterial population-level dynamics.

Based on the existing body of work on bacterial phenotyping, we wanted to optimize conditions and protocols to enable high-content bacterial phenotyping using an Opera Phenix (Perkin Elmer). The Opera Phenix is a dual spinning disk confocal microscope capable of acquiring images using four lasers and four cameras simultaneously, minimizing background fluorescence and time taken to capture images (Perkin Elmer). These features are vital for imaging bacteria because of their small size and the need to distinguish between individuals. In this study, we aimed to develop a methodology to simultaneously screen thousands of individual bacteria under a variety of conditions and further develop robust analysis pipelines to distinguish bacterial morphologies, following a consistent workflow (**Figure 3.1**).

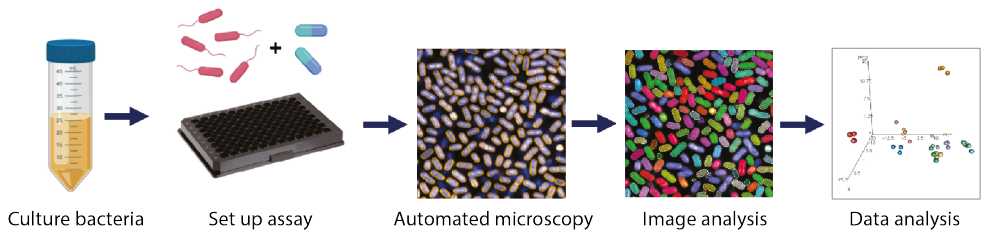

Figure 3.1 High content bacterial imaging and analysis workflow. A set of protocols was developed to culture bacteria, prepare samples for imaging, perform automatic microscopy and image analysis, and undertake analysis of the imaging data.

We further aimed to screen multiple bacterial isolates in tandem by comparing any morphological characteristics while growing in media or under challenge with antimicrobials. We hypothesized that it would be possible to distinguish between bacteria on the basis of their phenotypic characteristics after sufficient optimization of imaging and analysis parameters to specifically quantify trends in bacterial growth dynamics. We selected three distinct and clinically relevant bacterial species on which to optimize HCI and image analysis using the Opera Phenix: *Staphylococcus aureus* (Gram-positive), *Klebsiella pneumoniae* (Gram-negative, non-motile), and *Salmonella* Typhimurium (Gram-negative, motile). In line with the specific interest in *Salmonella* biology of the work described in this thesis and the particular challenges associated with imaging *Salmonella*, I undertook a more comprehensive optimization for *S*. Typhimurium, which will be the focus of this chapter.

3.2 Optimization of bacterial adhesion for imaging

Unlike low-throughput confocal microscopy, in which bacteria are typically placed on slides for single time point analysis, imaging on the Opera Phenix is conducted in 96- or 384-well plates. Thus, the first challenge was in optimizing the adhesion of bacteria, particularly motile ones, to the plastic ultra-thin-bottomed plates. Because motile *S*. Typhimurium D23580 did not adhere well to the plate plastic, we began by testing two types of thin-bottomed-plates, centrifuging *S.* Typhimurium D23580 bacteria onto the plates and exploring adhesion by coating plates with a variety of materials. Our initial panel of coatings included thin rat-tail collagen and *Salmonella*-specific antisera O4 and H:i to bind the surface lipopolysaccharide and/or flagella (**Figure 3.2**).

We found that although there were negligible visual differences between the two plate types (Cell Carrier versus Cell Carrier Ultra), it was necessary to coat the plates to have enough bacteria for imaging and analysis (**Figure 3.2 A, B**). Additionally, we found that initially, it was necessary to gently centrifuge *S*. Typhimurium D23580 bacteria onto the plates. However, none of the three initial well coatings bound sufficient numbers of bacteria for downstream visualization and analysis, so further optimization was required.

As bacterial adhesion was poor even with coating and centrifugation, we attempted to optimize other parts of the adhesion process. We hypothesized that fixation of motile bacteria

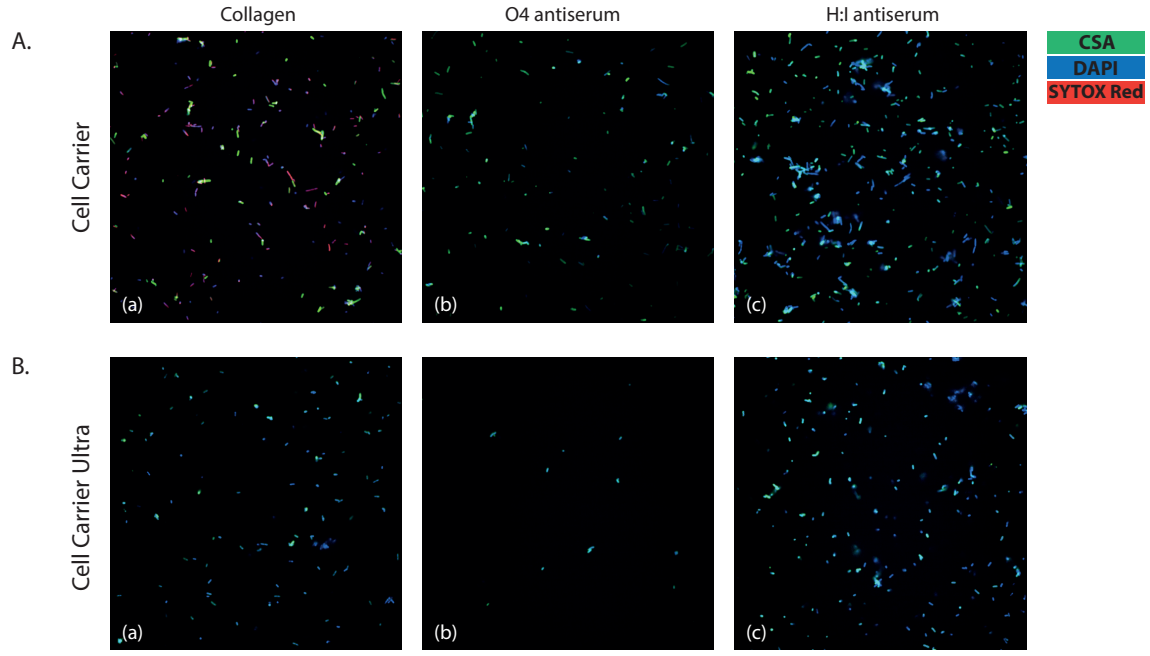

Figure 3.2 Comparison of Opera Phenix plates for *S*. Typhimurium imaging. Bacteria plated on Cell Carrier (**A**) or Cell Carrier Ultra (**B**) plates with coating of (a) collagen, (b) O4 antiserum or (c) H:i antiserum.

prior to addition to the plate might enhance adhesion because flagellar movement would be restricted. Thus, we compared bacteria fixed after plating and centrifugation (**Figure 3.3 A (a)**) with bacteria fixed in tubes and subsequently plated and centrifuged (**Figure 3.3 A (b)**).

However, this resulted in bacterial clumping, leading to blurred images. We next attempted to increase bacterial adhesion by centrifuging bacteria onto the plate at 4°C, hypothesizing that the bacteria would be less motile and therefore adhere better. Here, we centrifuged *S*. Typhimurium at either room temperature (**Figure 3.3 B (a)**) or at 4°C (**Figure 3.3 B (b)**). We found that while there was marginal improvement with centrifugation at 4°C, there were still very few bacteria in each field, and the image quality was poorer with the 4°C treatment.

Given the challenges associated with adhering *S*. Typhimurium to plates, we subsequently identified a set of 11 plate coatings that have previously been used to bind eukaryotic cells to surfaces[408–414]. We systematically screened binding of the three bacterial species of interest, including *S*. Typhimurium SL1344, to these coatings and compared the quality of images and number of adhered bacteria (**Figure 3.4, 3.5**).

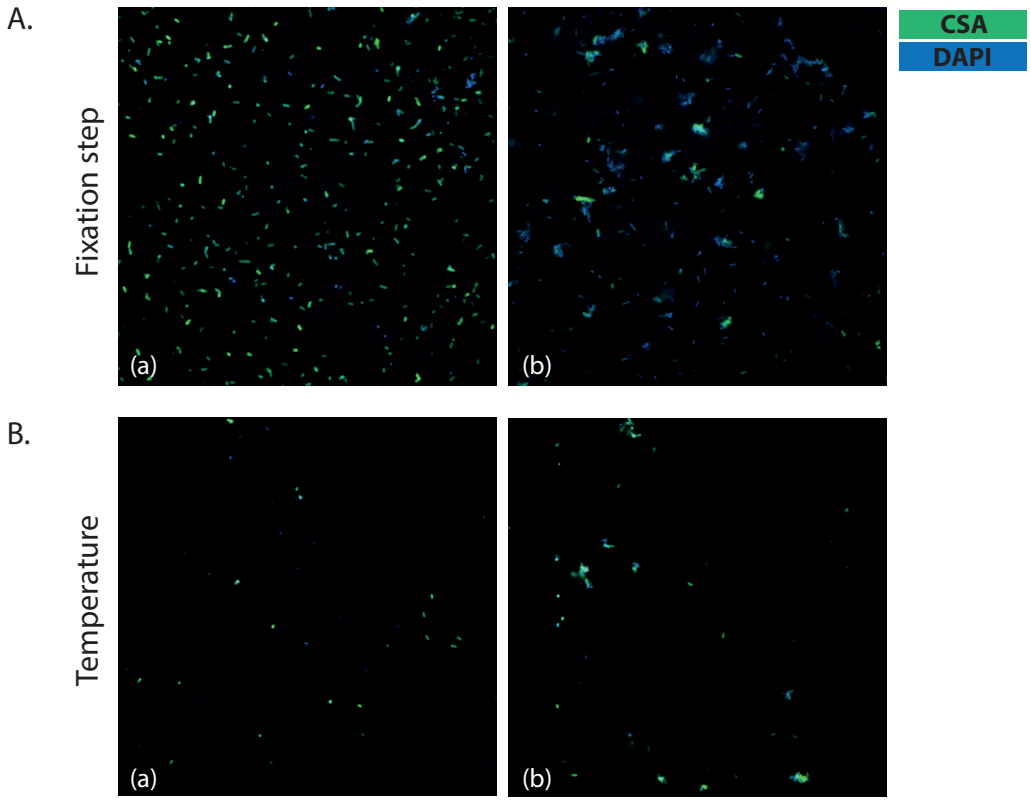

Figure 3.3 Optimization of fixation and temperature conditions for *S*. Typhimurium adhesion. All wells were coated with H:i antiserum prior to the addition of bacteria. **A.** Comparison of bacterial fixation with PFA before (a) or after (b) addition of bacteria to plates. **B.** Comparison of (a) bacteria centrifuged onto plates at room temperature or (b) at 4°C. Bacterial membranes are stained with CSA (green), and nucleic acids are stained with DAPI (blue).

Unsurprisingly, both isolates of *S*. Typhimurium tested adhered well to few coatings, possibly due to their motile nature. However, we found that *S*. Typhimurium could be successfully visualized and analysed after plates were coated with thick rat-tail collagen, Matrigel, or vitronectin (**Figure 3.5 B; Appendix B, Table B.1**). While these coating conditions were initially tested using *S*. Typhimurium SL1344, similar results were validated and confirmed for *S*. Typhimurium D23580 and other invasive *S*. Typhimurium isolates of interest. Based on the significant improvement in adhesion of *S*. Typhimurium with suitable coatings, it was then possible to develop and optimize next stages of the methodology.

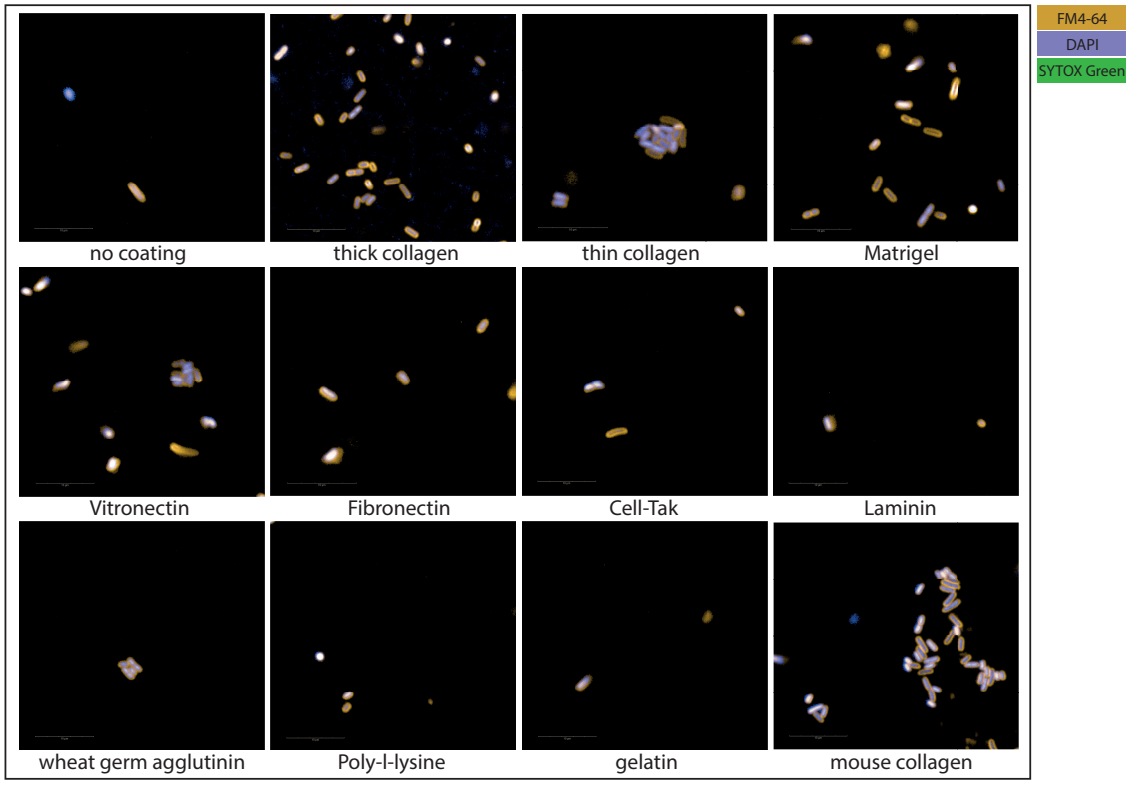

Figure 3.4 Comparison of *S.* Typhimurium SL1344 adhesion on 11 coatings and uncoated wells. Comprehensive optimization of *S.* Typhimurium adhesion to Cell Carrier Ultra wells coated with 11 alternative coatings and uncoated wells. Overnight cultures of *S.* Typhimurium bacteria were grown statically for 2 h in wells and then fixed, stained, and imaged.

3.3 Optimization of staining for *S.* Typhimurium

Following optimization of adhesion conditions, we wanted to evaluate and optimize staining protocols for all bacteria of interest and *S.* Typhimurium in particular. We based our initial fluorescent staining composition upon the work of Nonejuie *et al.*[359]. The stains were FM4-64, a cellular membrane stain; DAPI (4',6-diamidino-2-phenylindole), a membrane-permeable nucleic acid stain; and SYTOX Green, a membrane-impermeable nucleic acid stain. As SYTOX Green is membrane-impermeable, it is used as a readout for non-viable cells with ruptured membranes[415,416]. Upon staining with FM4-64, DAPI, and SYTOX Green, we found that while DAPI and SYTOX Green staining looked similar to those of images published by Nonejuie *et al.*, there was inconsistent surface staining of *S.* Typhimurium with FM4-64 (**Figure 3.6 A**)[359].

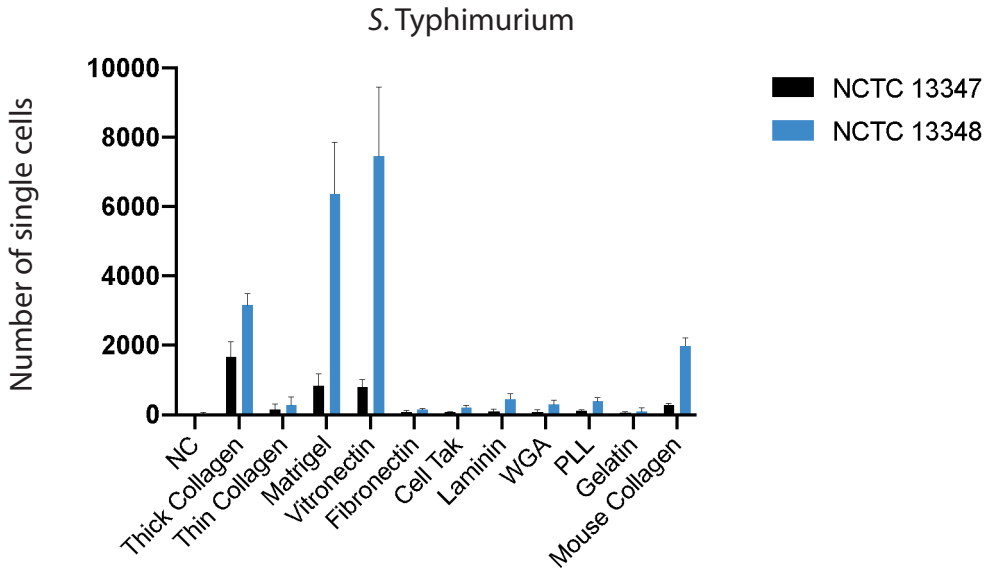

Figure 3.5 Quantification of bacterial single cells adhered to coated plates. Coatings were chosen for each bacterial isolate tested based on higher levels of adherent bacteria for two isolates of *S*. Typhimurium. The number of single cells was calculated using automated analysis by segmenting objects and identifying single cells.

We hypothesized that this may be due to inconsistent adhesion of *Salmonella* to wells or poorer integration of FM4-64 with the *Salmonella* cellular membrane. As a result, we next optimized staining with a FITC-conjugated *Salmonella*-specific antibody that binds the Common Structural Antigens (CSA) of multiple serotypes of *Salmonella* (**Figure 3.6 B**)[417]. As the CSA-FITC stain had the same excitation and emission spectra as SYTOX Green, we attempted to use SYTOX Red to measure dead cells. However, we found it difficult to optimize SYTOX Red concentrations, thus necessitating further stain optimization for *S*. Typhimurium. We subsequently found a CSA antibody conjugated to Alexa-647, which would allow for simultaneous use of SYTOX Green. Not only did this stain combination qualitatively produce the clearest staining of *S*. Typhimurium amongst the variations trialled, it also enabled us to compare directly between *S*. Typhimurium and other bacterial species using similar staining combinations (**Figure 3.6 C**).

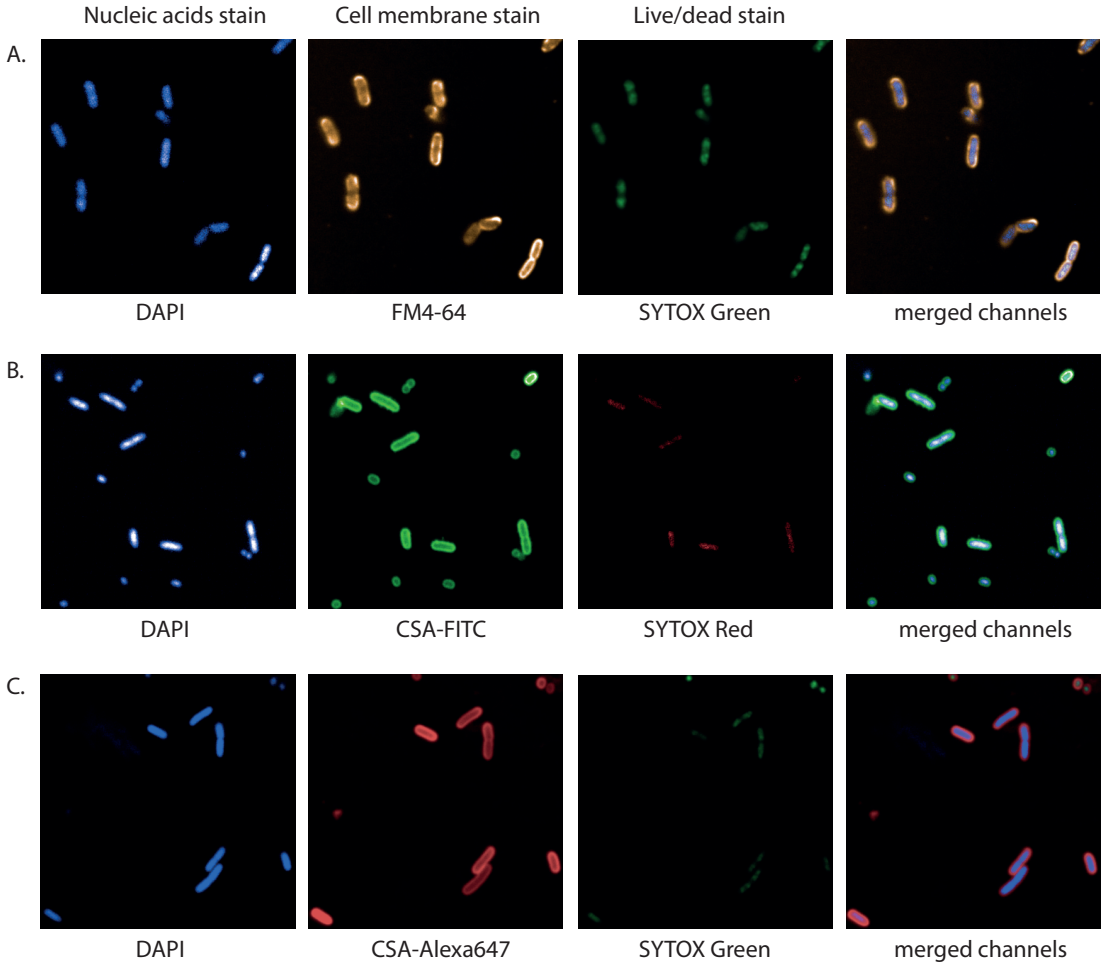

Figure 3.6 Optimization of staining for *S.* Typhimurium. A. Staining of *S.* Typhimurium using DAPI, FM4-64, and SYTOX Green as performed previously by Nonejuie *et al.*, 2013[359]. **B.** *Salmonella*-specific staining using CSA-FITC antibody to visualize outer membrane. **C.** Alternative *Salmonella*-specific staining using CSA-Alexa-647 antibody to visualize outer membrane.

3.4 Development of an *S.* Typhimurium analysis pipeline

Upon optimizing adhesion and staining protocols, we next developed analysis pipelines using the Harmony software by Perkin Elmer. A pipeline was developed specifically to measure less-adherent bacteria including *S.* Typhimurium. The pipeline inputted images taken on the Opera Phenix and then calculated the image data to distinguish objects of interest. Through a series of segmentation and selection steps, objects were refined based on size and other morphological parameters to be characterized as bacteria (**Figure 3.7; Appendix B, Table B.2**).

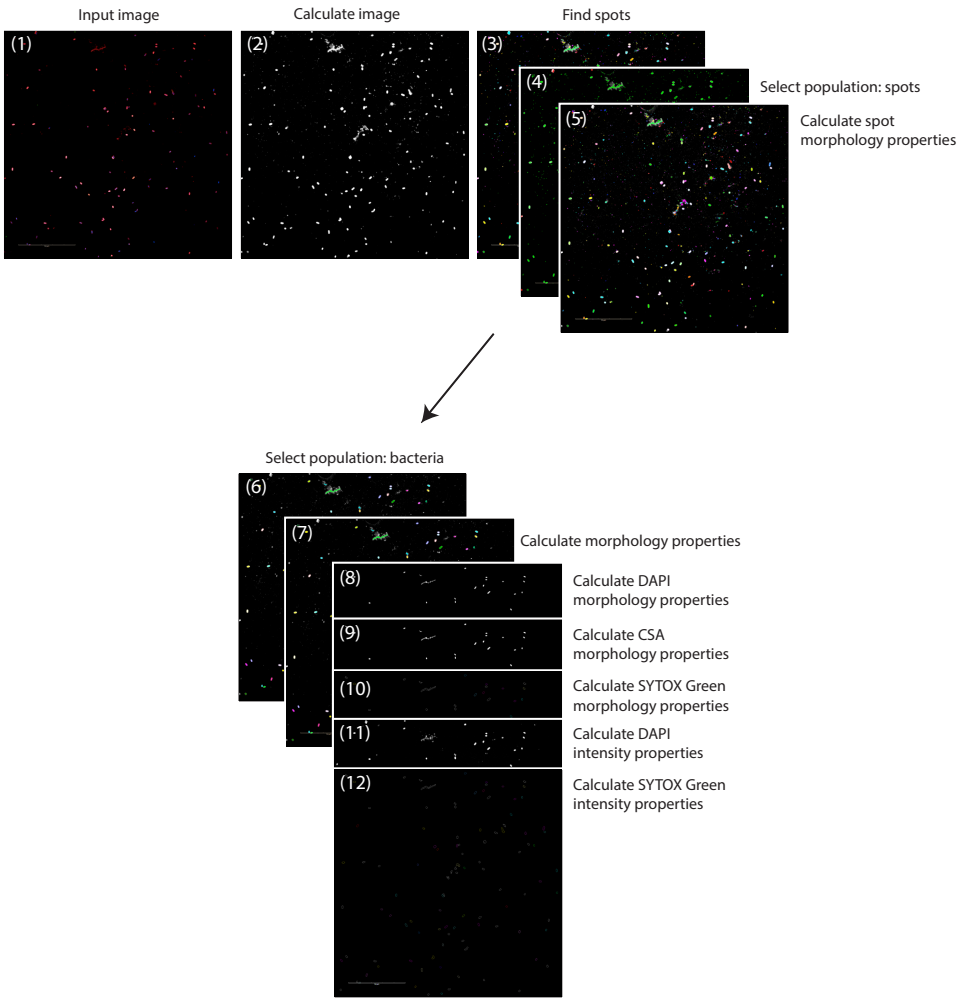

Figure 3.7 Analysis pipeline steps to identify and segment bacterial objects. Objects were calculated and measured from input images of *S.* Typhimurium (1) in a series of 12 steps prior to classification. Morphological and intensity properties were calculated based on overall objects and stains.

Various properties of the determined bacteria were calculated, including the morphological and intensity properties associated with each stain, as well as total morphology properties such as bacterial length and width (**Figure 3.7 (7)**). In addition to calculating more standard measurements, the Perkin Elmer Harmony software can also capture "STAR" morphologies, which calculate thresholds and weights of measurements to more precisely calculate fluorescence distribution, symmetry, and brightness (Perkin Elmer Image Analysis Technical Details). Upon selection of the "bacteria" population and characterization of the individual bacteria, a linear classifier was applied to distinguish between bacterial morphologies. We trained the linear classifier using a machine learning algorithm to identify the bacterial

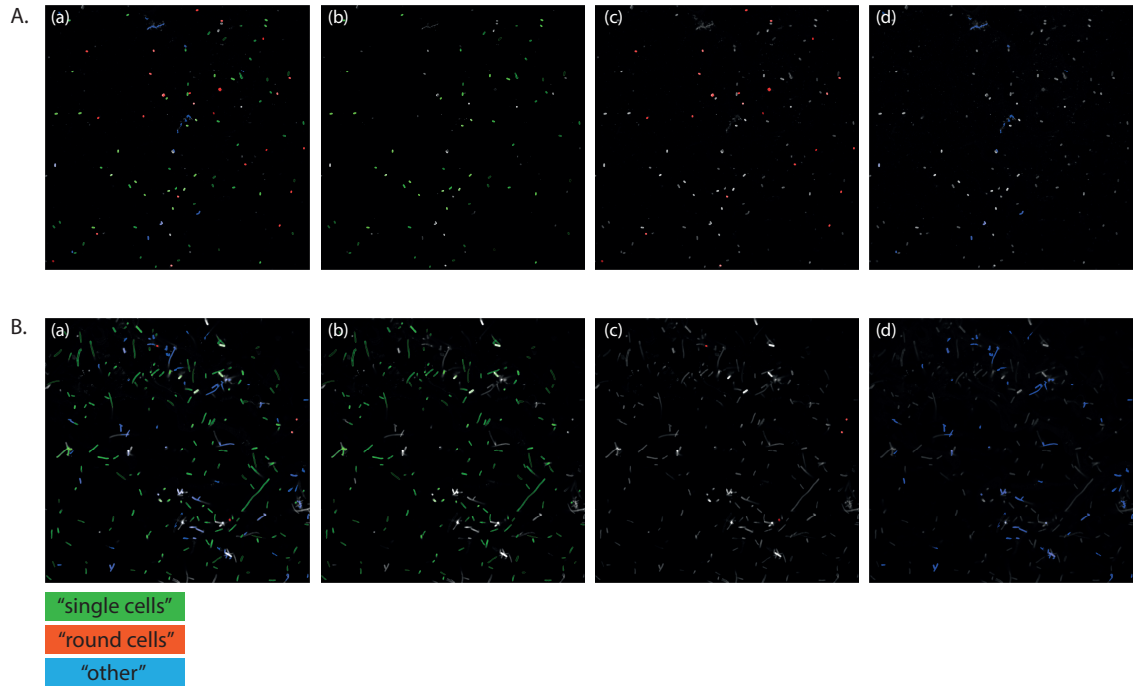

Figure 3.8 Linear classification of bacteria into three categories. A. Example of *S*. Typhimurium bacteria without antimicrobial treatment. **B.** *S*. Typhimurium bacteria under 2x MIC ciprofloxacin exposure. The linear classifier was trained to differentiate between objects in a field: all (a), "single cells" (b), "round cells" (c), and "other" (d) based on chosen morphologies of interest.

population as "single cells", "round cells", or "other". These categories were chosen based on visual scrutiny of the images and our interest in measuring morphological characteristics of single cells (**Figure 3.8**). Importantly, the linear classifier was robust enough to classify bacteria that had undergone morphological changes due to antimicrobial perturbation and still accurately distinguished between "single cells", "round cells", and "other" (**Figure 3.8 B**).

3.5 Imaging of antimicrobial-treated bacteria

We next wanted to test and validate imaging of bacteria perturbed by antimicrobial exposure. To do so, we selected a panel of nine clinically-relevant antimicrobials to *S*. Typhimurium bacteria with 5x MIC concentrations after assessment of antimicrobial susceptibility for each

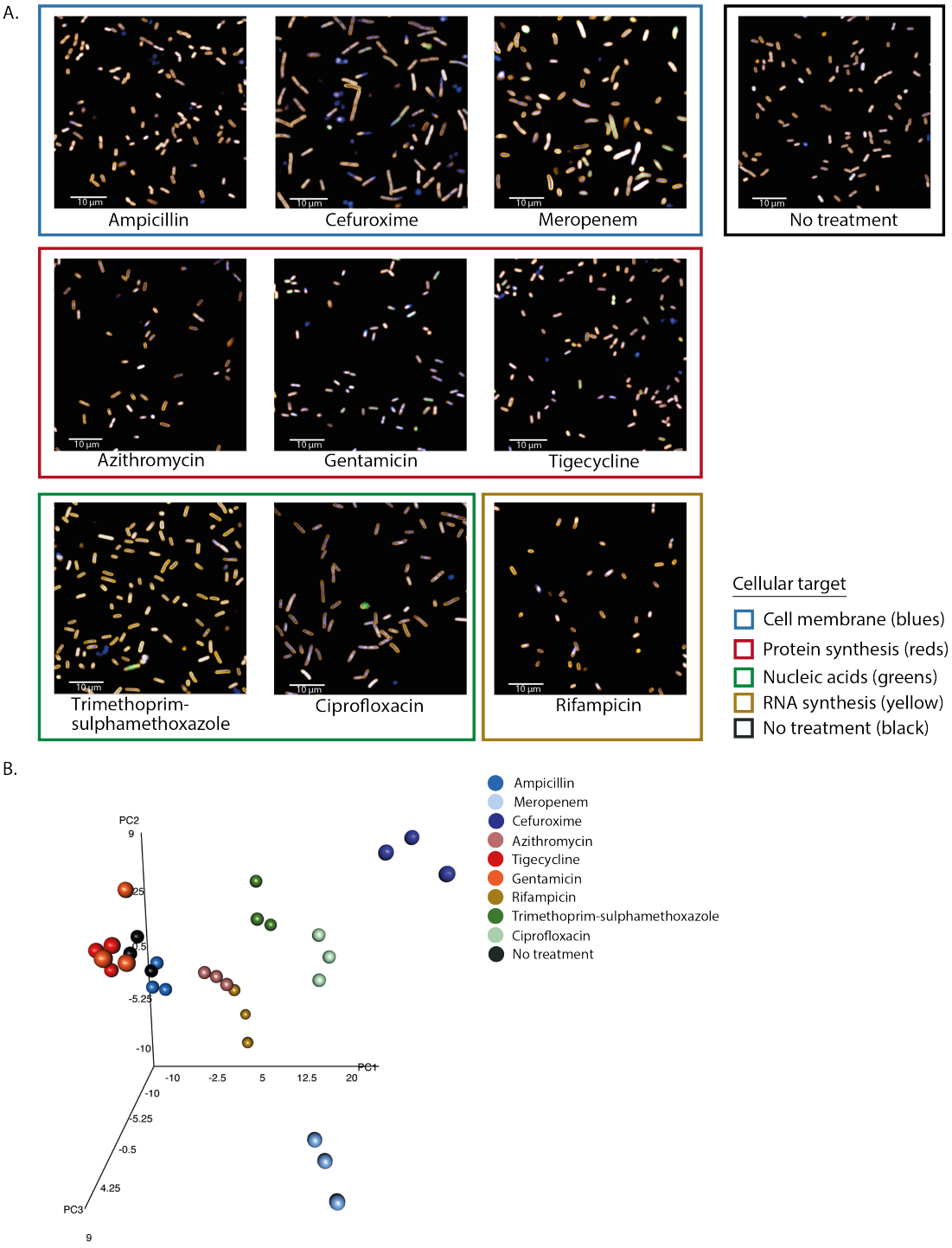

Figure 3.9 Phenotyping on the Opera Phenix of *S.* Typhimurium after 2 h antimicrobial exposure. A. Bacteria were imaged after exposure to 9 different antimicrobials for 2 h using DAPI (blue), FM4-64 (orange), and SYTOX Green (green). **B.** Principal component analysis showing clustering of technical replicates for each antimicrobial and separation between antimicrobial treatments based on morphological parameters.

isolate (**Appendix B, Table B.3**). This study was performed with triplicate wells of each antimicrobial treatment on each plate, and all experiments were done in biological triplicates to assess the consistency of the assay. We found that antimicrobials with different mechanisms of action were linked with different morphological changes to the bacteria (**Figure 3.9 A**). This was also validated by the clustering of the different antimicrobial-treated bacteria in a principal component analysis (**Figure 3.9 B**).

As we were particularly interested in changes to *S*. Typhimurium after ciprofloxacin exposure, we undertook further analysis to assess other bacterial characteristics. Visually, we could identify morphological differences between *S*. Typhimurium single bacteria treated with 0x, 1x, 2x or 4x MIC of ciprofloxacin for 2 h (**Figure 3.10 A**). We then plotted the number of bacteria measured at 2 h in each condition and found that there was considerable variation between bacterial numbers at this given time point (**Figure 3.10 B**). This may have been due to differences in optical densities of the bacterial cultures after 2 h growth. Importantly, there were more than 500 single bacteria per treatment, providing an adequate number of cells to perform further analysis on. We were also interested in performing downstream analysis on only the live bacteria, as distinguished by SYTOX Green fluorescence. This was one of the parameters measured in the automated analysis, and we graphed the density distribution of SYTOX Green mean fluorescence intensity of the total bacterial population at 2 h (**Figure 3.10 C**). We found that while there was not a clean bimodal distribution of fluorescence clearly delineating "live" versus "dead" bacteria, there was the highest density of bacteria with low SYTOX Green fluorescence and a diminishing tail of increasing fluorescence.

To further discriminate between live and dead bacteria, we drew an arbitrary and conservative threshold where the density of bacteria decreased (**Figure 3.10 C**). We called bacteria to the left of this threshold "live" and those to the right "dead" for downstream analysis of the live population. While some live bacteria may have been included in the "dead" bin, we decided that it was better to exclude some "live" bacteria than include "dead" bacteria in further analysis. To guide downstream analysis, we were curious to know what parameters were deemed important for any given treatment condition. To achieve this, we accessed *Z*' (z-prime) statistics for ciprofloxacin-treated versus non-treated *S*. Typhimurium. Interestingly, many of the highest-ranked *Z*' parameters were staining parameters that were not visually discernible; however, they likely influenced clustering of the different antimicrobial treated bacteria in the PC plot (**Figure 3.9; Table 1; Appendix B, Table B.4**).

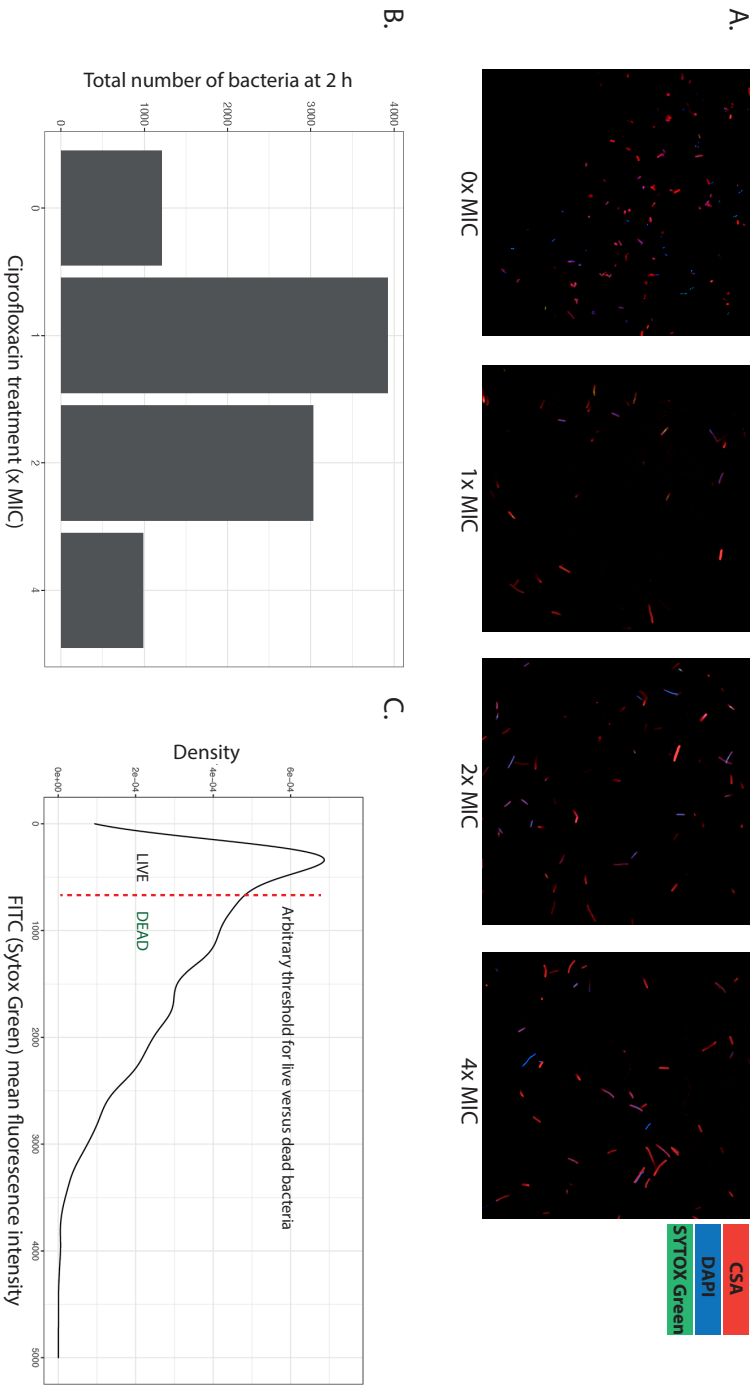

Figure 3.10 Assessment of ciprofloxacin-treated *S.* Typhimurium after Opera Phenix imaging. **A.** Images from *S.* Typhimurium treated with either 0x, 1x, 2x, or 4x MIC of ciprofloxacin for 2 h. **B.** Quantification of total number of analysed bacteria from Perkin Elmer Harmony analysis software. **C.** Analysis of SYTOX Green mean fluorescence intensity at 2 h over all bacteria to measure distribution. An arbitrary cut-off of ∼750 AU was applied to threshold live bacteria.

Table 3.1 *Z'*-statistics for the 20 most important parameters to distinguish between ciprofloxacin-treated (2x MIC) and non-treated *S*. Typhimurium.

Parameter	Z'
CSA Symmetry 14 - StdDev per Well	0.953
CSA Symmetry 04 - StdDev per Well	0.953
CSA Symmetry 15 - Mean per Well	0.938
DAPI Symmetry 15 - Mean per Well	0.935
CSA Symmetry 04 - Mean per Well	0.934
CSA Radial Relative Deviation - Mean per Well	0.933
CSA Symmetry 02 - Mean per Well	0.93
CSA Symmetry 12 - Mean per Well	0.921
CSA Symmetry 14 - Mean per Well	0.918
CSA Threshold Compactness 60% - Mean per Well	0.918
CSA Threshold Compactness 40% - Mean per Well	0.917
CSA Axial Length Ratio - Mean per Well	0.916
CSA Threshold Compactness 30% - Mean per Well	0.913
CSA Radial Mean - Mean per Well	0.9
CSA Threshold Compactness 50% - Mean per Well	0.897
Roundness - Mean per Well	0.896
Spot Roundness - Mean per Well	0.896
DAPI Symmetry 14 - StdDev per Well	0.893
DAPI Threshold Compactness 60% - Mean per Well	0.891
Length [µm] - Mean per Well	0.889

3.6 Discussion

In this study, we developed a methodology to perform HCI and subsequent automated image analysis on individual *S*. Typhimurium bacteria grown in liquid culture using an Opera Phenix high-throughput confocal microscope. We were able to apply this technique to systematically screen large numbers of *S*. Typhimurium exposed to a variety of antimicrobials and could use morphological parameters determined by image analysis to discriminate between antimicrobial treatments.

Despite the clear advantages of HCI to screen bacteria, development of this methodology exposed some of the challenges associated with HCI of individual bacteria. Imaging in 96-well plates enables rapid and efficient screening of bacteria under multiple treatments in parallel, introducing experimental flexibility and ability to collect vast amounts of single-cell data. However, our study illustrated that the acquisition of such information requires extensive

optimization of imaging to have sufficient numbers and quality of bacteria to perform image analysis. We developed our assay based on existing methodologies for lower-throughput imaging, and we found numerous challenges associated with imaging *S*. Typhimurium[359].

The most significant challenge in imaging *S*. Typhimurium was adhesion of bacteria to the plastic wells, which we ascribed to the motility and outer membrane composition of the bacteria. It is anticipated that similar challenges would occur for other motile bacteria, although we did not validate our methodology on alternative motile bacterial species. There was a high degree of variability in adhesion of *S*. Typhimurium to uncoated wells, and overall number of adhered bacteria was low. While there was marginal improvement with *S*. Typhimurium-specific coatings of O4 and H:i antisera, it was interesting that both of those coatings diminished image quality. It may be that the specific binding of the antisera occluded the binding of stain or caused bacterial aggregation, thus worsening the fluorescent signal[418–420]. We found that the most-suitable well coatings for *S*. Typhimurium in terms of image quality and number of adherent cells were compounds often used for stem cell adhesion to plastics.

Upon optimization of coating conditions, it was still necessary to optimize staining conditions for *S*. Typhimurium. Once again, this may have been due to the outer membrane composition of *S*. Typhimurium or that insufficient adhesion of bacteria to wells impacted staining efficacy. In this case, there was a clear advantage to the use of *Salmonella*-specific outer membrane CSA, which yielded brighter and more compact staining of the bacterial membranes. The use of a *Salmonella*-specific stain may also be advantageous in the future when studying interactions of bacteria with host cells. The optimization of SYTOX staining to identify dead cells was important because this allows for more nuanced downstream analysis of live and dead bacterial populations[421,422]. In this study, we did not perform analysis on live versus dead cells; however, the inclusion of the STYOX stain enabled discrimination of antimicrobial mechanisms of action in our principal component analysis of antimicrobial-treated bacteria. Moreover, we were able to plot the density of SYTOX staining across a bacterial population and draw a threshold of SYTOX fluorescence intensity to discriminate between potentially live and dead cells. It is important to recognize that some studies have found incongruity between membrane rupture and cell viability depending on DNA topology and degradation, which may confound interpretation of SYTOX fluorescence intensity[423–425]. Nevertheless, SYTOX intensity may be an important feature in future analyses, particularly when looking at bacterial sub-populations within a well displaying different characteristics.

Adequate imaging of *S*. Typhimurium facilitated screening of bacteria for the development of an automated analysis pipeline that could capture a large number of morphological parameters. In the context of bacteria treated with a panel of antimicrobials, this set of parameters could then be used to perform a principal component analysis to discriminate between bacteria treated with antimicrobials with different mechanisms of action. The value of this methodology is that it can be applied in a multitude of contexts: to predict the mechanisms of action of novel compounds, measure killing efficacy of a panel of drugs, and compare morphological differences between related organisms, among others. The development of high content screening of individual bacteria opens up a multitude of possibilities to explore and characterize the diversity of bacterial phenotypes.